

Nonperturbative improvement of stout-smear three-flavor clover fermions

N. Cundy,¹ M. Göckeler,¹ R. Horsley,² T. Kaltenbrunner,¹ A. D. Kennedy,² Y. Nakamura,^{1,3} H. Perlt,⁴ D. Pleiter,³ P. E. L. Rakow,⁵ A. Schäfer,¹ G. Schierholz,^{1,6} A. Schiller,⁴ H. Stüben,⁷ and J. M. Zanotti²

(QCDSF-UKQCD Collaboration)

¹*Institut für Theoretische Physik, Universität Regensburg, 93040 Regensburg, Germany*

²*School of Physics and Astronomy, University of Edinburgh, Edinburgh EH9 3JZ, United Kingdom*

³*Deutsches Elektronen-Synchrotron DESY, 15738 Zeuthen, Germany*

⁴*Institut für Theoretische Physik, Universität Leipzig, 04109 Leipzig, Germany*

⁵*Theoretical Physics Division, Department of Mathematical Sciences, University of Liverpool, Liverpool L69 3BX, United Kingdom*

⁶*Deutsches Elektronen-Synchrotron DESY, 22603 Hamburg, Germany*

⁷*Konrad-Zuse-Zentrum für Informationstechnik Berlin, 14195 Berlin, Germany*

(Received 11 February 2009; published 27 May 2009)

We discuss a three-flavor lattice QCD action with clover improvement in which the fermion matrix has single level stout smearing for the hopping terms together with unsmeared links for the clover term. With the (tree-level) Symanzik improved gluon action this constitutes the stout link nonperturbative clover or SLiNC action. To cancel $O(a)$ terms the clover term coefficient has to be tuned. We present here results of a nonperturbative determination of this coefficient using the Schrödinger functional and as a by-product a determination of the critical hopping parameter. Comparisons of the results are made with lowest order perturbation theory.

DOI: [10.1103/PhysRevD.79.094507](https://doi.org/10.1103/PhysRevD.79.094507)

PACS numbers: 12.38.Gc

I. INTRODUCTION

When constructing a lattice QCD action, even the simplest gluon action has only $O(a^2)$ corrections. The naive quark action also has $O(a^2)$ corrections, but suffers from the “doubling problem” describing 16 flavors in the continuum limit. A cure is to add the Wilson mass term, so 15 flavors decouple in the continuum limit, but the price is that there are now $O(a)$ corrections (and also loss of chiral invariance), so that, for example, for a ratio of hadron masses

$$\frac{m_H}{m_{H'}} = r_0 + ar_1 + O(a^2). \quad (1)$$

The Symanzik approach is a systematic improvement to $O(a^n)$ (where in practice $n = 2$ for the fermion action) by adding a basis (an asymptotic series) of irrelevant operators and tuning their coefficients to completely remove $O(a^{n-1})$ effects. Restricting improvement to on-shell quantities the equations of motion reduce the set of operators in both the action and in matrix elements. Indeed, for $O(a)$ improvement of the fermion action only one additional flavor-singlet operator is required

$$\mathcal{L}_{\text{clover}} \propto ac_{\text{sw}} \sum_{q,x,\mu\nu} \bar{q}(x) \sigma_{\mu\nu} F_{\mu\nu}(x) q(x), \quad (2)$$

the so-called “Sheikholeslami-Wohlert” or “clover” term, [1]. So if we can improve *one* on-shell quantity this then fixes c_{sw} as a function of the lattice spacing a or equivalently of the bare coupling g_0^2 , so that all other on-shell quantities are automatically improved to $O(a)$, i.e., we now

have

$$\frac{m_H}{m_{H'}} = r_0 + O(a^2). \quad (3)$$

A nonperturbative determination of c_{sw} will be the main goal of this paper, the general approach being described below.

Matrix elements still require additional $O(a)$ operators, for example, for the axial current and pseudoscalar density [2],¹

$$\begin{aligned} \mathcal{A}_\mu &= (1 + b_A am_q)(A_\mu + c_A a \partial_\mu^{\text{LAT}} P), \\ \mathcal{P} &= (1 + b_P am_q)P, \end{aligned} \quad (4)$$

(for mass degenerate quarks) with

$$A_\mu = \bar{q} \gamma_\mu \gamma_5 q, \quad P = \bar{q} \gamma_5 q, \quad (5)$$

which require additional b_A , c_A , and b_P improvement coefficients. An easily determined quantity is the quark mass computed from the partially conserved axial current Ward identity (PCAC WI),²

$$m_q^{\text{WI}} = \frac{\langle \partial_0^{\text{LAT}}(A_0(x_0) + c_A a \partial_0^{\text{LAT}} P(x_0)) O \rangle}{2 \langle P(x_0) O \rangle}. \quad (6)$$

¹We implicitly distinguish between quark flavors in operators, i.e., consider nonsinglet operators.

² $\partial_\mu^{\text{LAT}}$ is the symmetric lattice derivative, $(\partial_\mu^{\text{LAT}} f)(x) = [f(x + a\hat{\mu}) - f(x - a\hat{\mu})]/(2a)$, and (no μ summation), $(\partial_\mu^{2\text{LAT}} f)(x) = [f(x + a\hat{\mu}) - 2f(x) + f(x - a\hat{\mu})]/a^2 = (\partial_\mu^{\text{LAT}} \partial_\mu^{\text{LAT}} f)(x) + O(a^2)$.

Choosing different operators, O , gives different determinations of the quark mass $m_q^{\text{WI}(i)}$, $i = 1, 2$ with different lattice artifacts. If the quark mass is improved then its errors are $O(a^2)$. So we can determine the “optimal” c_{sw} improvement coefficient by tuning until

$$m_q^{\text{WI}(1)} = m_q^{\text{WI}(2)}. \quad (7)$$

[This is equivalent to considering the renormalized quark mass

$$m_{qR} = \frac{Z_A(1 + b_A a m_q)}{Z_P(1 + b_P a m_q)} m_q^{\text{WI}}. \quad (8)$$

In general the b_A, b_P coefficients do affect considerations of $O(a)$ improvement. However, here one imposes a condition at fixed bare parameters (g_0^2, m_q) which means that the factors drop out.] Practically, how this is achieved will be discussed in this paper after the action is introduced.

This paper is organized as follows. In Sec. II, the action is given and in Sec. III the Schrödinger functional is briefly discussed, together with the general procedure for determining the optimal c_{sw} and optimal critical hopping parameter, κ_c . Section IV gives some lattice details for a series of simulations at various coupling constants, which after suitable interpolations leads to this determination. Section V then discusses possible finite size effects in the results. Results are collected together in Sec. VI and a polynomial interpolation (in the coupling constant) for both c_{sw} and κ_c is given, together with a comparison with the lowest order perturbation result. Finally in Sec. VII some brief conclusions are discussed. Tables of the raw results are given in the Appendix.

II. THE SLINC ACTION

We shall consider here $n_f = 3$ flavor stout link clover fermions—SLiNC fermions (stout link nonperturbative clover). In a little more detail, for each flavor,

$$S_F = \sum_x \left\{ \kappa \sum_\mu [\bar{q}(x)(\gamma_\mu - 1)\tilde{U}_\mu(x)q(x + a\hat{\mu}) - \bar{q}(x)(\gamma_\mu + 1)\tilde{U}_\mu^\dagger(x - a\hat{\mu})q(x - a\hat{\mu})] + \bar{q}(x)q(x) - \frac{1}{2}\kappa a c_{\text{sw}} \sum_{\mu\nu} \bar{q}(x)\sigma_{\mu\nu} F_{\mu\nu}(x)q(x) \right\}. \quad (9)$$

Rescaling the quark fields $q \rightarrow q/\sqrt{2\kappa}$ gives the quark mass m_q where

$$m_q(c_{\text{sw}}) = \frac{1}{2a} \left(\frac{1}{\kappa} - \frac{1}{\kappa_c(c_{\text{sw}})} \right), \quad (10)$$

which is proportional to the PCAC quark mass, m_q^{WI} . The loss of chiral invariance means that for a given c_{sw} a critical hopping parameter, $\kappa_c(c_{\text{sw}})$ has now also to be determined.

The hopping terms (Dirac kinetic term and Wilson mass term, i.e., those terms involving a κ) in Eq. (9) use a once

stout-smear link or “fat link,” [3],

$$\tilde{U}_\mu = \exp\{iQ_\mu(x)\}U_\mu(x),$$

$$Q_\mu(x) = \frac{\alpha}{2i}[VU^\dagger - UV^\dagger - \frac{1}{3}\text{Tr}(VU^\dagger - UV^\dagger)], \quad (11)$$

(V_μ is the sum of all staples around U_μ) while the clover term remains built from “thin” links—they are already of length $4a$ and we want to avoid the fermion matrix becoming too extended. Smearing is thought to help at present lattice spacings by smoothing out fluctuations in the gauge fields slightly and so reducing the condition number and also to avoid a near first-order phase transition. The critical kappa in Eq. (10) corresponds to an additive mass renormalization

$$m_c(c_{\text{sw}}) = \frac{1}{2a} \left(\frac{1}{\kappa_c(c_{\text{sw}})} - \frac{1}{1/8} \right). \quad (12)$$

It is known that with a combination of link fattening and increase of the clover coefficient, it is possible to reduce this mass term [4–6]. The stout variation is also analytic which means that the derivative in the gauge group can be taken (so the force in the hybrid Monte Carlo, or HMC, simulation is well defined) and perturbative expansions are also possible, [7].

To complete the action we also use the Symanzik tree-level gluon action

$$S_G = \frac{6}{g_0^2} \left\{ c_0 \sum_{\text{Plaquette}} \frac{1}{3} \text{Re Tr}(1 - U_{\text{Plaquette}}) + c_1 \sum_{\text{Rectangle}} \frac{1}{3} \text{Re Tr}(1 - U_{\text{Rectangle}}) \right\}, \quad (13)$$

together with

$$c_0 = \frac{20}{12}, \quad c_1 = -\frac{1}{12}, \quad \text{and} \quad \beta = \frac{6c_0}{g_0^2} = \frac{10}{g_0^2}. \quad (14)$$

While this gluon action has elements of higher order improvement, namely $O(a^4)$, this is not the reason that it is used here. [The best we can hope for the fermion action is $O(a^2)$ improvement.] Again we wish to move the action away from a nearby first-order phase transition occurring when using the standard Wilson action (i.e., $c_0 \rightarrow 1, c_1 \rightarrow 0$) [8], by using a slightly extended action. Different values of c_0 and c_1 can be and have been used in the literature to address this problem, e.g., [8].

III. THE SCHRÖDINGER FUNCTIONAL

The ALPHA Collaboration determined the improvement coefficients by means of the “Schrödinger functional,” [2,9–11]. Some numerical results for c_{sw} for the quenched case ($n_f = 0$) were given in [12,13], for $n_f = 2$ flavors in [14] and for $n_f = 3$ flavors in [15–17]. In this approach Dirichlet boundary conditions are applied on the time boundaries to the fields. For the gluon fields, fixing them

on the boundary is then equivalent to inducing some classical background field about which they fluctuate. It is simplest to consider spatially constant color diagonal fields, corresponding to a constant chromo-electric background field. Concretely, we consider a $L^3 \times T$ lattice (with $T = 2L$) and take the background field to be

$$U_0^c(\vec{x}, x_0) = 1, \quad (15)$$

$$U_k^c(\vec{x}, x_0) = \exp\left(-i\frac{a}{T}[x_0 C^{(2)} + (T - x_0)C^{(1)}]\right),$$

with

$$C^{(i)} = \frac{1}{L} \begin{pmatrix} \phi_1^{(i)} & 0 & 0 \\ 0 & \phi_2^{(i)} & 0 \\ 0 & 0 & \phi_3^{(i)} \end{pmatrix}, \quad (16)$$

and

$$(\phi_1^{(1)}, \phi_2^{(1)}, \phi_3^{(1)}) = \left(-\frac{1}{6}\pi, 0, \frac{1}{6}\pi\right), \quad (17)$$

$$(\phi_1^{(2)}, \phi_2^{(2)}, \phi_3^{(2)}) = \left(-\frac{5}{6}\pi, \frac{1}{3}\pi, \frac{1}{2}\pi\right),$$

and fix the boundary values *a posteriori*. As we have an extended gauge action (rather than the simpler Wilson gluon action), we fix two values at each double boundary layer and so we choose, following [18],³ U_μ^c from Eq. (15) at $x_0 = -a, 0$ (lower boundary) and similarly U_μ^c at $x_0 = T - a$ and T (upper boundary). The ‘‘bulk’’ of the lattice is thus from $x_0 = 0$ to $x_0 = T - a$. Additionally the weight factors for the gluon loops in Eq. (14) must be appropriately chosen on the boundary for $O(a)$ improvement. Classically these weight factors are not difficult to find, however a full nonperturbative determination would be difficult. But away from the boundaries, they only affect the local PCAC relation to $O(a^2)$ and so are not essential for the determination of the optimal c_{sw} , and so it is sufficient to use the classical values.

The fixed boundary quark fields, $\rho, \bar{\rho}$ (taken as zero here) make simulations with $m_q \sim 0$ with no zero mode problems possible. They are specified on the lower inner boundary and upper inner boundary from

$$P_0^+ q(\vec{x}, 0) = \rho^{(1)}(\vec{x}), \quad \bar{q}(\vec{x}, 0)P_0^- = \bar{\rho}^{(1)}(\vec{x}),$$

$$P_0^- q(\vec{x}, T - a) = \rho^{(2)}(\vec{x}), \quad \bar{q}(\vec{x}, T - a)P_0^+ = \bar{\rho}^{(2)}(\vec{x}), \quad (18)$$

where P_0^\pm is the projection operator defined by

$$P_0^\pm = \frac{1}{2}(1 \pm \gamma_0). \quad (19)$$

These projections are necessary for consistency. ρ and $\bar{\rho}$ can be taken as sinks and sources, respectively, to build

³An alternative procedure using single layer boundaries is given in [19].

operators for correlation functions. For example, here we can take at the lower inner boundary $x_0 = 0$ ($i = 1$) and upper inner boundary $x_0 = T - a$ ($i = 2$), the operators

$$O^{(i)} = \sum_{\vec{y}, \vec{z}} \left(-\frac{\delta}{\delta \rho^{(i)}(\vec{y})}\right) \gamma_5 \left(\frac{\delta}{\delta \bar{\rho}^{(i)}(\vec{z})}\right). \quad (20)$$

So we can investigate PCAC behavior at different distances from the boundaries.

In a little more detail, following Eq. (6), we first set

$$r^{(i)}(x_0) = \frac{\partial_0^{\text{LAT}} f_A^{(i)}(x_0)}{2f_P^{(i)}(x_0)}, \quad s^{(i)}(x_0) = a \frac{\partial_0^{2\text{LAT}} f_P^{(i)}(x_0)}{2f_P^{(i)}(x_0)}, \quad (21)$$

where

$$f_A^{(1)}(x_0) = -\frac{1}{n_f^2 - 1} \langle A_0(x_0) O^{(1)} \rangle,$$

$$f_A^{(2)}(T - x_0) = +\frac{1}{n_f^2 - 1} \langle A_0(x_0) O^{(2)} \rangle, \quad (22)$$

and

$$f_P^{(1)}(x_0) = -\frac{1}{n_f^2 - 1} \langle P(x_0) O^{(1)} \rangle,$$

$$f_P^{(2)}(T - x_0) = -\frac{1}{n_f^2 - 1} \langle P(x_0) O^{(2)} \rangle. \quad (23)$$

Then redefine the quark mass slightly, but which coincides to $O(a^2)$ for the improved theory

$$M^{(i)}(x_0, y_0) = r^{(i)}(x_0) + \hat{c}_A(y_0) s^{(i)}(x_0),$$

$$\hat{c}_A(y_0) = -\frac{r^{(1)}(y_0) - r^{(2)}(y_0)}{s^{(1)}(y_0) - s^{(2)}(y_0)}, \quad (24)$$

which eliminates the unknown c_A in the determination of the quark mass [12], and replaces it by an estimator, \hat{c}_A . Improvement is defined when

$$(M, \Delta M) = (0, 0), \quad (25)$$

where

$$M \equiv M^{(1)}, \quad \Delta M \equiv M^{(1)} - M^{(2)}, \quad (26)$$

are chosen at some suitable x_0 , [12]. This gives the required optimal c_{sw} and κ_c , which we will denote by a star: c_{sw}^* and κ_c^* . Conventionally, we choose

$$M \equiv M^{(1)}(T/2, T/4), \quad (27)$$

$$\Delta M \equiv M^{(1)}(3T/4, T/4) - M^{(2)}(3T/4, T/4).$$

There are small changes due to the finite volume used, so Eq. (25) becomes

$$(M, \Delta M) = (0, \Delta M^{\text{tree}}), \quad (28)$$

where ΔM^{tree} is the tree-level (i.e., $g_0^2 = 0$, $c_{\text{sw}} \equiv c_{\text{sw}}^{\text{tree}} = 1$) value of $\Delta M|_{M=0}$ on the $L^3 \times T$ lattice. This ensures that $c_{\text{sw}} \rightarrow 1$ exactly as $\beta \rightarrow \infty$. For $\alpha = 0$, the analytic

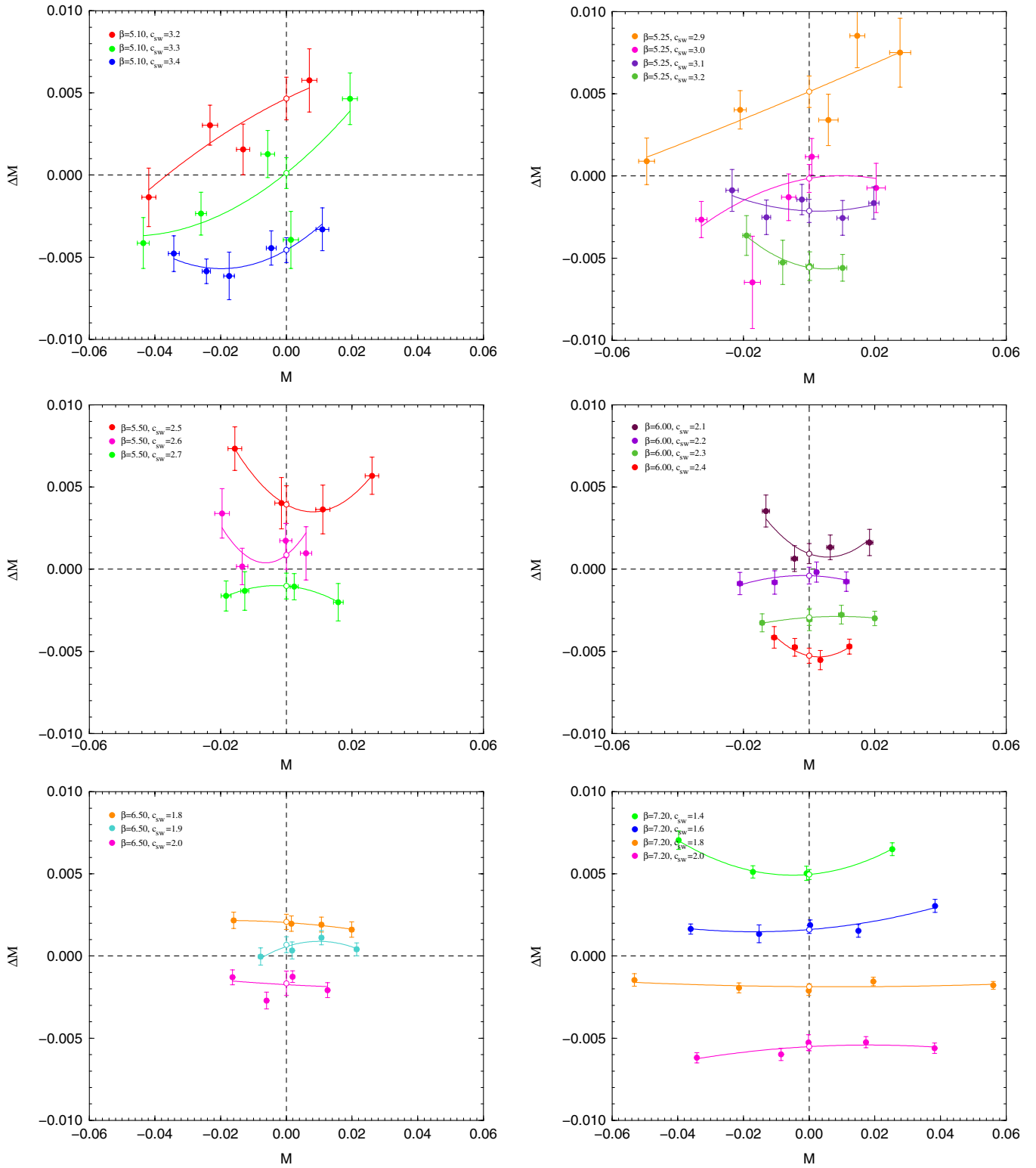


FIG. 1 (color online). ΔM against M for $\beta = 5.10, 5.25$ (upper left, right pictures, respectively), for $\beta = 5.50, \beta = 6.00$ (middle left, right pictures, respectively), and for $\beta = 6.50, \beta = 7.20$ (lower left, right pictures, respectively), together with quadratic interpolations to $M = 0$ (the open symbols).

result on a $N_s^3 \times 2N_s = 8^3 \times 16$ lattice (where $L = aN_s$) is 0.000277, [12]. Carrying out the interpolation procedures outlined in the next section for a free configuration, with background field given by Eq. (15) yields 0.000271. For the stout smearing used here (see next section) we find this is reduced to $\Delta M^{\text{tree}} = 0.000066$ and so we have neglected ΔM^{tree} in the following and simply used Eq. (25).

IV. THE LATTICE SIMULATION

The three-flavor lattice simulation used the Chroma software library [20], the Schrödinger functional details following [18]. Results were mostly generated on $N_s^3 \times 2N_s \equiv 8^3 \times 16$ lattices, together with some additional $12^3 \times 24$ lattices, using the HMC algorithm together with the RHMC variation [21] for the one-flavor. A mild smearing of $\alpha = 0.1$ was used. A series of simulations

were performed [typically generating $O(3000)$ trajectories for the $8^3 \times 16$ lattices and $O(2000)$ trajectories for the $12^3 \times 24$ lattices], quadratic and then linear interpolations of the $(M, \Delta M)$ results being used to locate the optimal point $(0, 0)$ as described below. Some further details and tables of the results are given in the Appendix. (Preliminary results were given in [22].)

A. c_{sw}^*

We have a two-parameter interpolation in c_{sw} and κ which is split here into two separate interpolations. First plotting ΔM against M and then interpolating to $M = 0$ for fixed c_{sw} gives a critical κ , namely, $\kappa_c(c_{\text{sw}})$,

$$\Delta M(c_{\text{sw}}, \kappa)|_{M=0} \equiv \Delta M(c_{\text{sw}}, \kappa_c(c_{\text{sw}}))|_{M=0} \equiv \Delta M(c_{\text{sw}}). \quad (29)$$

In Figs. 1 and 2 we plot ΔM versus M for various c_{sw}

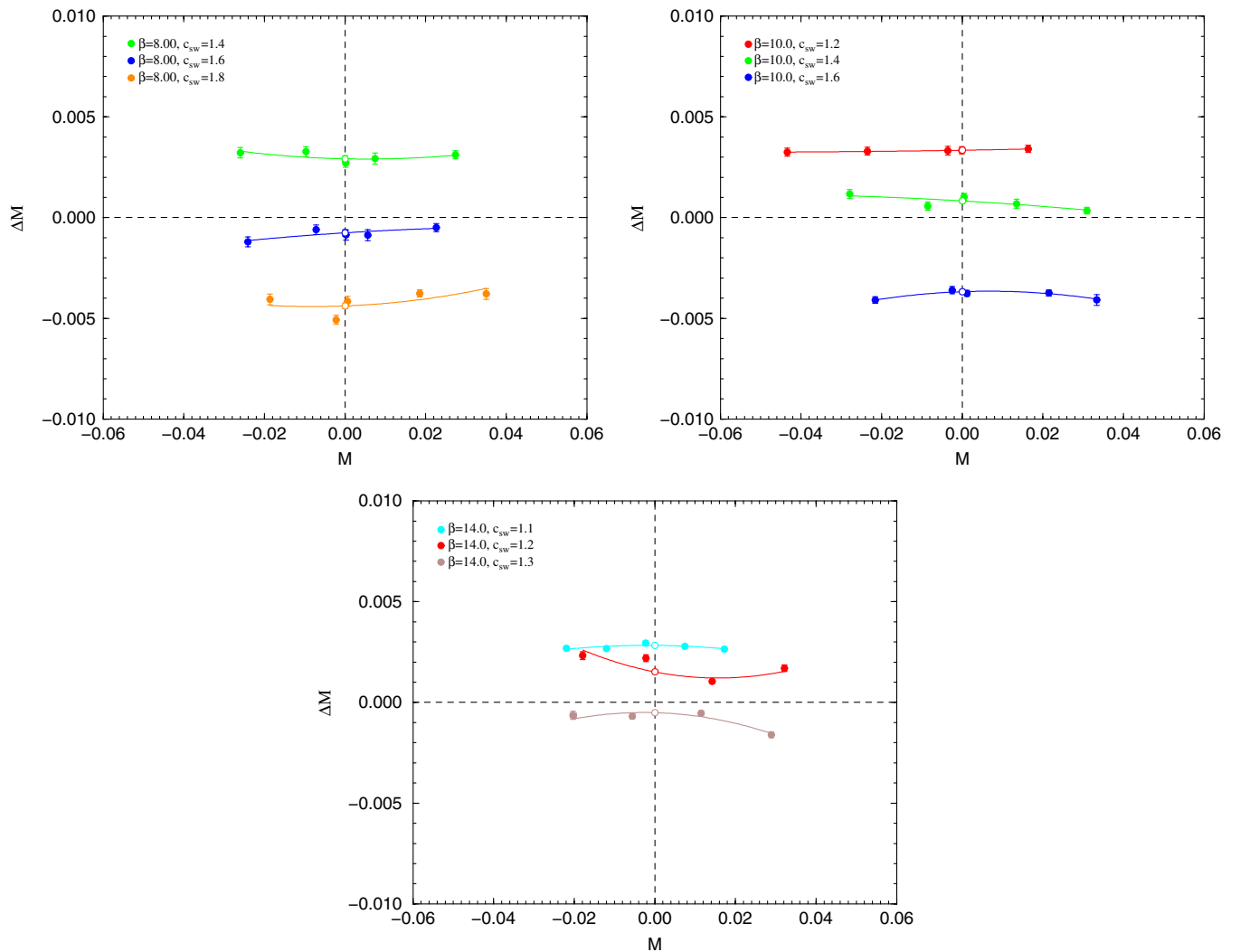


FIG. 2 (color online). ΔM against M for $\beta = 8.00, 10.0$ (upper left, right pictures, respectively) and for $\beta = 14.0$ (lower picture), together with quadratic interpolations to $M = 0$ (the open symbols).

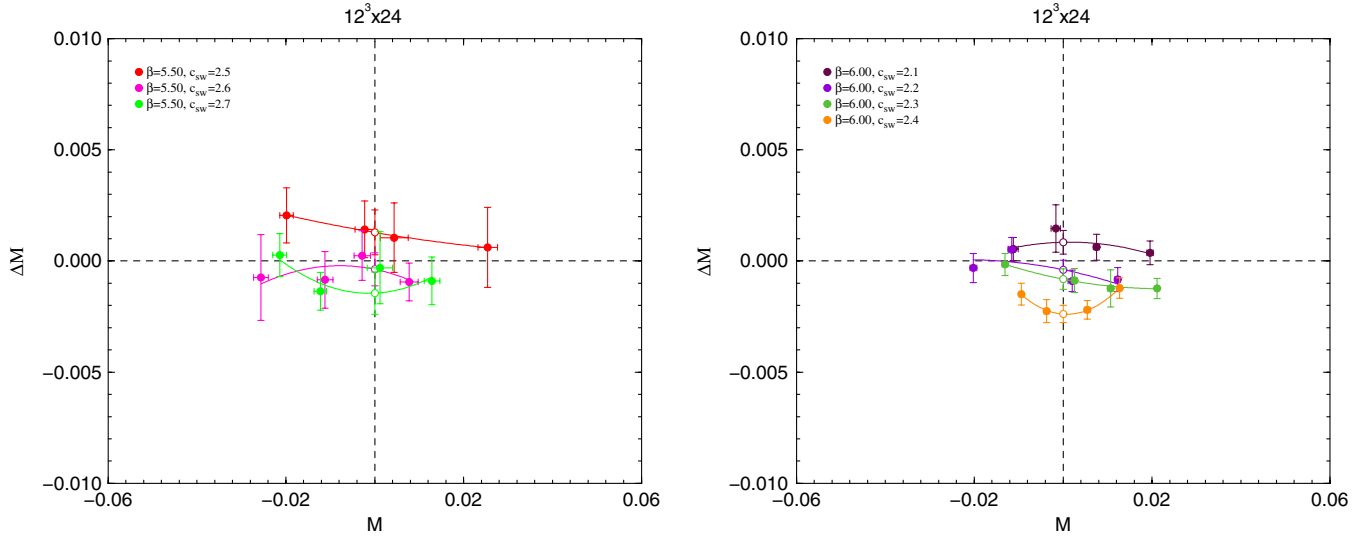


FIG. 3 (color online). ΔM against M for $\beta = 5.50, 6.00$ (left, right pictures, respectively) on a $12^3 \times 24$ lattice together with quadratic interpolations to $M = 0$ (the open symbols).

values for the $8^3 \times 16$ lattices and in Fig. 3 the results for the $12^3 \times 24$ lattices.

These graphs are the fundamental plots requiring high statistics as ΔM is the difference between two different M 's. As there are always 4 (or more) points for each graph a quadratic fit is made and the value of ΔM is determined where M vanishes.

These values of $\Delta M(c_{sw})$ for each β value are then plotted against c_{sw} as shown in Fig. 4 together with linear fits. The point where $\Delta M(c_{sw})$ vanishes gives c_{sw}^* . This gives values of

$$c_{sw}^* = \left\{ \begin{array}{ll} 3.302(13) & \beta = 5.10 \\ 3.030(13) & \beta = 5.25 \\ 2.651(23) & \beta = 5.50 \\ 2.163(17) & \beta = 6.00 \\ 1.915(10) & \beta = 6.50 \\ 1.690(07) & \beta = 7.20 \\ 1.559(05) & \beta = 8.00 \\ 1.407(04) & \beta = 10.0 \\ 1.279(06) & \beta = 14.0 \end{array} \right\} 8^3 \times 16 \quad (30)$$

$$\left\{ \begin{array}{ll} 2.584(38) & \beta = 5.50 \\ 2.181(28) & \beta = 6.00 \end{array} \right\} 12^3 \times 24$$

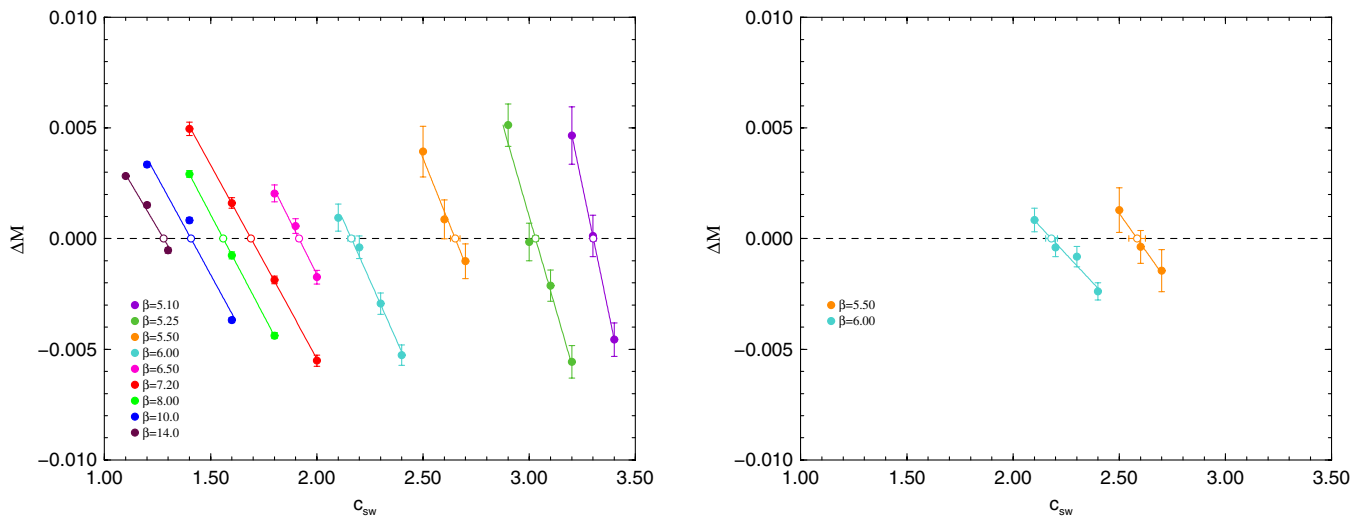


FIG. 4 (color online). ΔM at $M = 0$ against c_{sw} for various values of β (filled circles) together with linear interpolations to $\Delta M = 0$ (open circles). The left plot shows the $8^3 \times 16$ results while the right plot shows the $12^3 \times 24$ results.

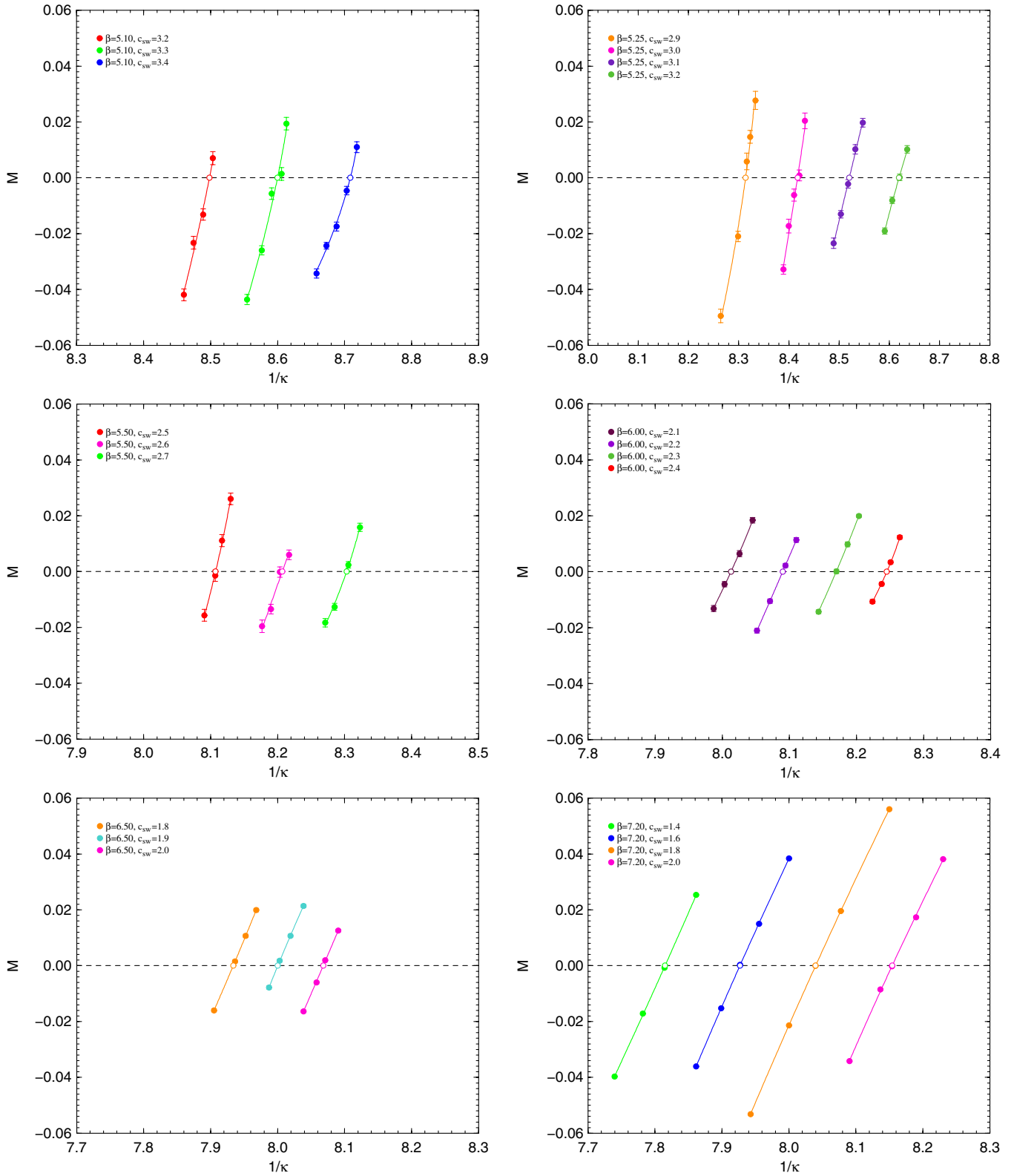


FIG. 5 (color online). M against $1/\kappa$ for $\beta = 5.10, 5.25$ (upper left, right pictures, respectively), for $\beta = 5.50, \beta = 6.00$ (middle left, right pictures, respectively), and for $\beta = 6.50, \beta = 7.20$ (lower left, right pictures, respectively), together with quadratic interpolations to $M = 0$ (the open symbols).

We postpone a discussion of possible finite size effects until Sec. V.

From Fig. 4, we see that linear fits even for four points (the $\beta = 7.20, 6.00, 5.25$ results) show very little curvature, so that we may write [14]

$$\Delta M(c_{sw}) = \omega(c_{sw} - c_{sw}^*), \quad (31)$$

with the gradient, ω , a slowly varying function of g_0 . To test this we note that

$$\frac{\partial \Delta M(c_{sw})}{\partial c_{sw}} = \omega, \quad (32)$$

so a fit to the gradients in Fig. 4 (for the $8^3 \times 16$ lattices) yields an estimate for ω . We find that ω is constant with an approximate value of -0.018 , although for the largest values of g_0^2 there are deviations from this.

B. κ_c^*

A similar procedure yields κ_c^* : plotting M against $1/\kappa$ and interpolating quadratically to $M = 0$ for fixed c_{sw} gives the critical κ , denoted by $\kappa_c(c_{sw})$. Then subsequently plotting $\Delta M(c_{sw})$ against $1/\kappa_c(c_{sw})$ and interpolating using a linear fit to $\Delta M = 0$ gives κ_c^* .

We first plot M against $1/\kappa$ for the $8^3 \times 16$ results in Figs. 5 and 6 and for the $12^3 \times 24$ results in Fig. 7.

Note that to produce these graphs should not require high statistics as it does not involve ΔM . [Although these are not the fundamental graphs they are also useful in helping to determine the various (c_{sw}, κ) values for the runs.]

These $\Delta M(\kappa_c)$ are then plotted in Fig. 8 again with a linear fit. Where ΔM vanishes gives κ_c^* . For legibility the results have been split into subgraphs. We see that κ_c^* is a nonmonotonic function of β .

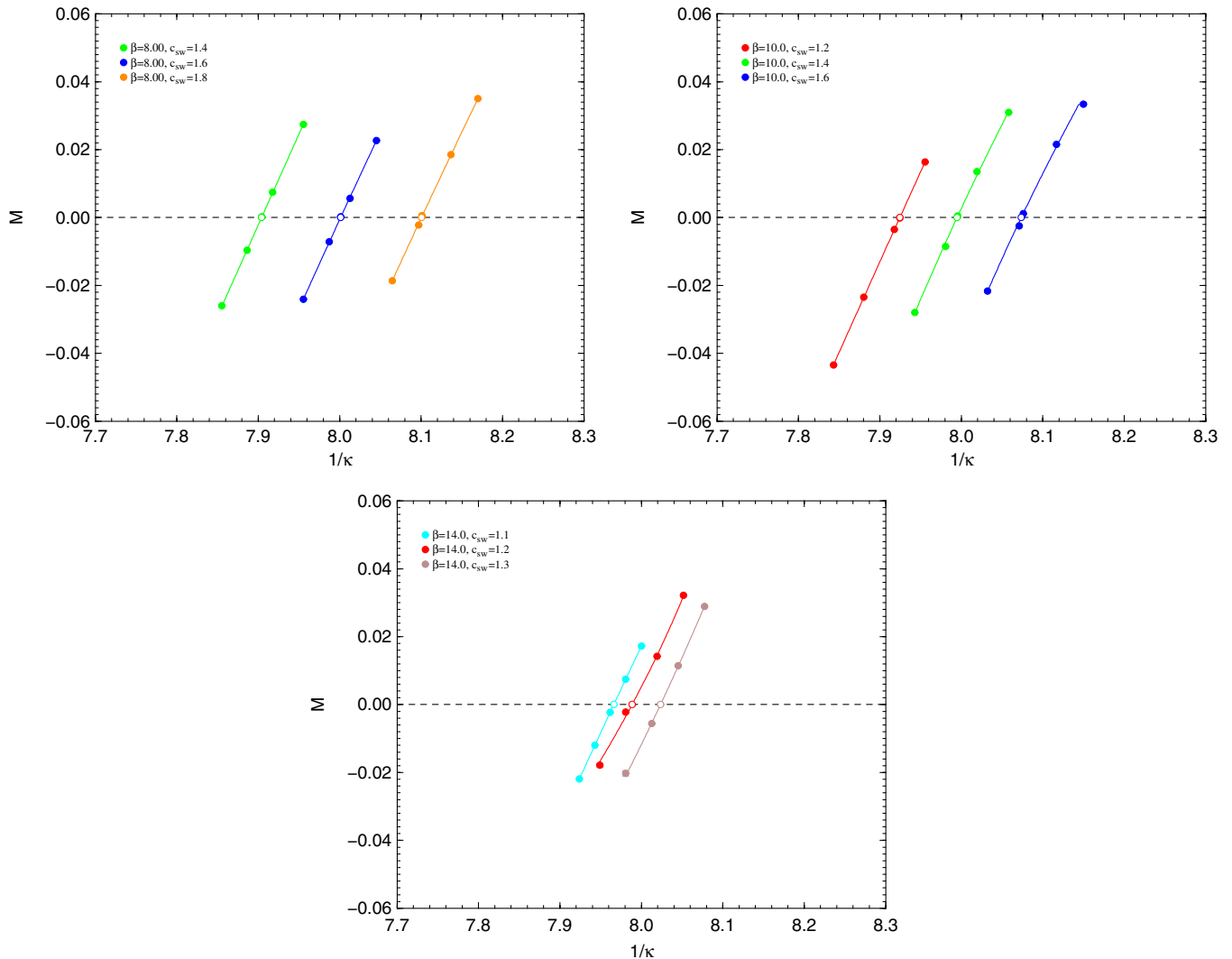


FIG. 6 (color online). M against $1/\kappa$ for $\beta = 8.00, 10.0$ (upper left, right pictures, respectively) and for $\beta = 14.0$ (lower picture), together with quadratic interpolations to $M = 0$ (the open symbols).

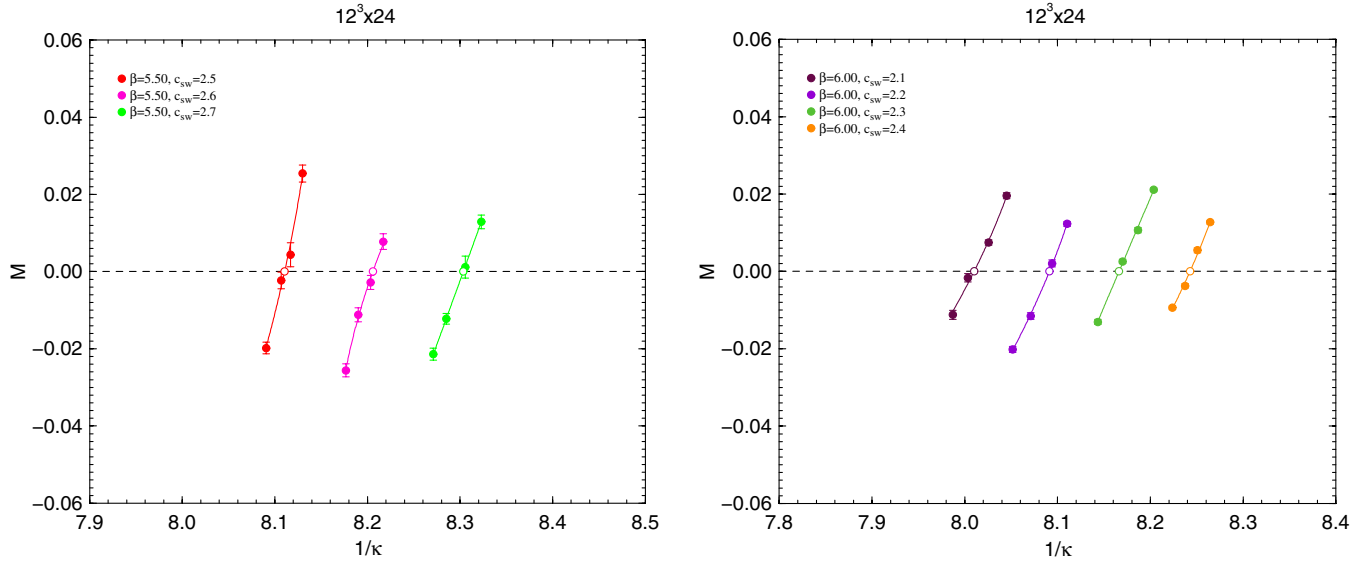


FIG. 7 (color online). M against $1/\kappa$ for $\beta = 5.50, 6.00$ (left, right pictures, respectively) on a $12^3 \times 24$ lattice together with quadratic interpolations to $M = 0$ (the open symbols).

We find results of

$$\kappa_c^* = \left\{ \begin{array}{ll} 0.116\,227(180) & \beta = 5.10 \\ 0.118\,385(184) & \beta = 5.25 \\ 0.121\,125(330) & \beta = 5.50 \\ 0.124\,043(199) & \beta = 6.00 \\ 0.124\,825(107) & \beta = 6.50 \\ 0.125\,343(61) & \beta = 7.20 \\ 0.125\,281(38) & \beta = 8.00 \\ 0.124\,993(22) & \beta = 10.0 \\ 0.124\,773(26) & \beta = 14.0 \end{array} \right\}_{8^3 \times 16} \quad (33)$$

$$\left\{ \begin{array}{ll} 0.122\,086(554) & \beta = 5.50 \\ 0.123\,849(330) & \beta = 6.00 \end{array} \right\}_{12^3 \times 24}$$

As a consistency check the alternative plot of c_{sw} against $1/\kappa_c$ is shown in Fig. 9 where c_{sw} is plotted against $1/\kappa_c(c_{sw})$, again with a linear fit between the points. The optimal values of c_{sw} , namely c_{sw}^* , taken from the previous fits as given in Eq. (30) are shown as dashed horizontal lines, the intersection with the $1/\kappa_c$ curves then giving the optimal critical values of κ_c , namely κ_c^* . These are denoted in the figure as open points. As a comparison, the results from the previous determination of κ_c^* , Eq. (33), are also shown as vertical lines. We see good agreement between the different determinations of κ_c^* , which indicates that the fit procedure adopted here gives consistent results for both

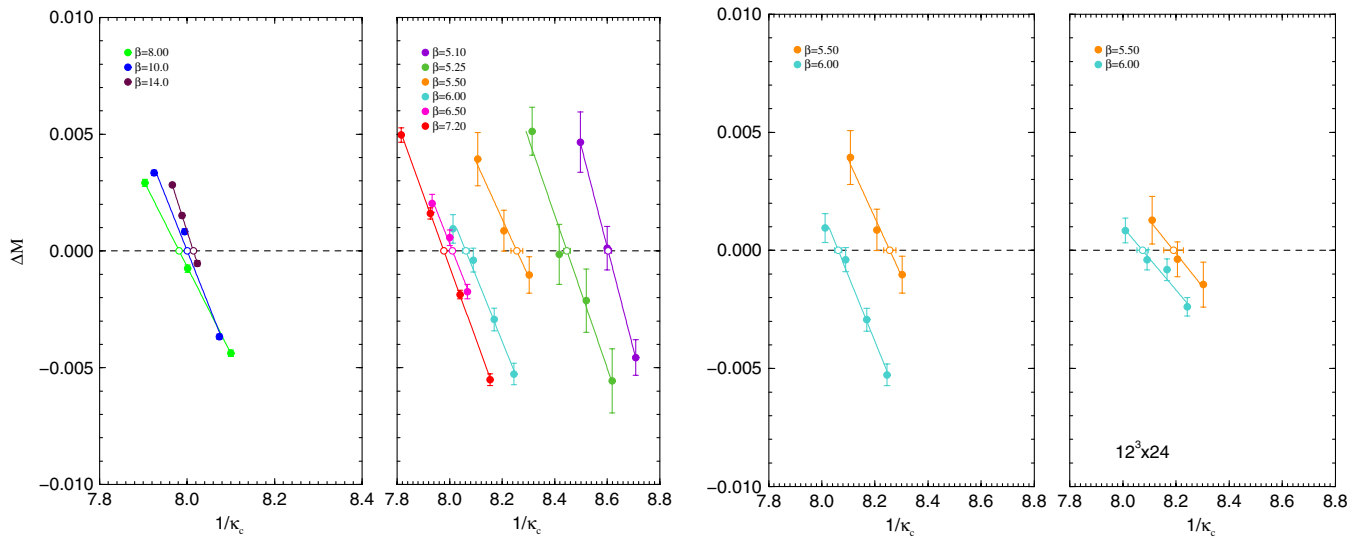


FIG. 8 (color online). Results of $\Delta M(\kappa_c(c_{sw}))$ versus $1/\kappa_c$ together with linear fits. The open circles give the optimal critical κ_c^* 's, i.e., the κ_c^{*} 's. The two left plots show the $8^3 \times 16$ results while the two right plots compare the $\beta = 5.50, 6.00$, $8^3 \times 16$ results with the $12^3 \times 24$ results.

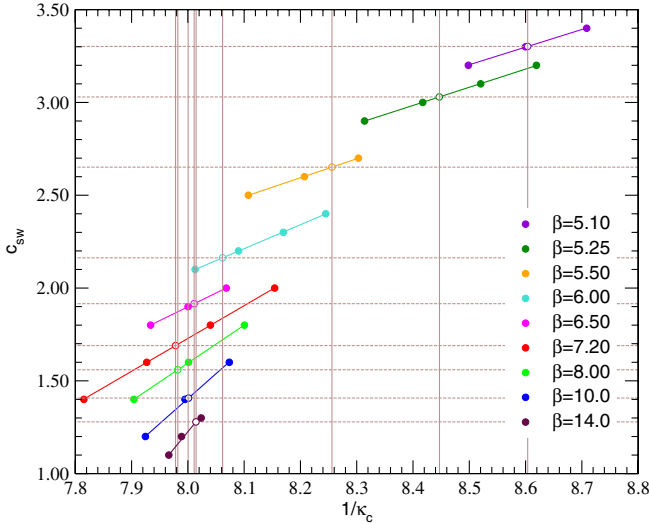


FIG. 9 (color online). Results of c_{sw} (filled circles) versus $1/\kappa_c$ together with linear fits. The optimal c_{sw} , c_{sw}^* , from Eq. (30) are shown as dashed horizontal lines. The open circles are the intersection of the linear fits with these horizontal lines and give an alternative determination of the optimal critical κ_c , κ_c^* , which are to be compared with the results of Eq. (33) shown as vertical lines.

c_{sw}^* and κ_c^* . Finally note that plotting the $n_f = 2$ flavor results would yield a similar curve to Fig. 9.

For future reference (in Sec. VI B) as the fits in Fig. 9 are all linear, then we write

$$\frac{1}{\kappa_c} = \frac{1}{\kappa_c^*} + d(c_{\text{sw}} - c_{\text{sw}}^*), \quad (34)$$

with a measured coefficient $d(g_0)$,

$$d = \left[\begin{array}{cc} 1.0521(92) & \beta = 5.10 \\ 1.0208(54) & \beta = 5.25 \\ 0.9783(100) & \beta = 5.50 \\ 0.7753(53) & \beta = 6.00 \\ 0.6722(51) & \beta = 6.50 \\ 0.5658(11) & \beta = 7.20 \\ 0.4907(10) & \beta = 8.00 \\ 0.3719(08) & \beta = 10.0 \\ 0.2704(23) & \beta = 14.0 \end{array} \right] 8^3 \times 16. \quad (35)$$

V. FINITE SIZE EFFECTS

There are (small) ambiguities due to the finite volume used. In an infinite volume we expect $O(a\Lambda_{\text{QCD}})$ contributions [in the chiral limit, otherwise there are also extra $O(am_q)$ terms] due to the different boundary conditions or operators chosen. In a finite volume there are additional $O(a/L)$ terms. Thus, one might expect asymptotically, following [16],

$$c_{\text{sw}}^*(g_0, L/a) = c_{\text{sw}}^*(g_0, \infty) + c_L \frac{a}{L} + c_\Lambda a\Lambda_{\text{QCD}} + \dots \quad (36)$$

The terms proportional to $a\Lambda_{\text{QCD}}$ vanish as a (or g_0^2) $\rightarrow 0$ and represent the ambiguities in the different definitions of M . For a physical quantity \mathcal{Q} , then

$$\begin{aligned} \mathcal{Q} &= \mathcal{Q}(a) + q_L(c_{\text{sw}}^*(g_0, L/a) \\ &\quad - c_{\text{sw}}^*(g_0, \infty))a\Lambda_{\text{QCD}} + O(a^2) \\ &= \mathcal{Q}(a) + q_L c_L \frac{a}{L} a\Lambda_{\text{QCD}} + O(a^2). \end{aligned} \quad (37)$$

The correction term may be rewritten as (where $L = aN_s$)

$$q_L c_L \frac{a}{L} a\Lambda_{\text{QCD}} = \frac{q_L c_L}{N_s} a\Lambda_{\text{QCD}}. \quad (38)$$

Potentially this might mean that \mathcal{Q} is no longer $O(a)$ improved for simulations where c_{sw}^* has been determined on a fixed lattice size, N_s . However, it is likely that the unknown coefficients q_L and c_L are small and coupled with the N_s factor in the denominator, this is then expected to be a small effect.

To avoid this altogether we can either keep L fixed in physical units as $a \rightarrow 0$ (the ‘‘constant physics condition’’) so $O(a/L) \rightarrow 0$, or alternatively simulate for several values of N_s and extrapolate to $N_s \rightarrow \infty$. The ‘‘poor man’s solution’’ is to evaluate at large $\beta \rightarrow \infty$ (i.e., on a free configuration for $N_s = 8$ here) and subtract this result. Practically, following the same procedure as in Sec. IV A we have found that for c_{sw} this $O(1/N_s)$ term (for $N_s = 8$) is negligible.

As noted previously we have also performed additional simulations on larger lattices $12^3 \times 24$ for $\beta = 6.00, 5.50$ in order to discuss finite lattice size corrections. The results are plotted in Figs. 3 and 7, and compared with the $8^3 \times 16$ results in Figs. 4 and 8. At tree level we have [23]

$$\Delta M^{\text{tree}} = k(c_{\text{sw}}^{\text{tree}} - 1) \frac{a}{L} + \dots, \quad (39)$$

which would indicate that for larger N_s then ΔM becomes smaller, with the consequent noise/signal ratio becoming worse. Indeed this is seen in our results, with the $12^3 \times 24$ data being more bunched together in Fig. 3 than for the corresponding $8^3 \times 16$ data in Fig. 1. This may be mitigated somewhat by choosing a larger range of c_{sw} due to the linear nature of the data as seen in Fig. 4 and Eq. (31). For $\beta = 6.00$ we have increased the number of c_{sw} ’s used in the analysis.

In Fig. 10 we plot c_{sw}^* and κ_c^* against $1/N_s$. For both $\beta = 6.00$ and 5.50 there seems to be small finite size effects for c_{sw}^* . For κ_c^* this is also the case for $\beta = 6.00$, while for $\beta = 5.50$ the situation is perhaps a little less clear-cut. However, there is no systematic trend in the data and a constant fit always lies within the error bars of the data. So although we cannot come to a definite conclusion, there do not seem to be large finite volume effects, i.e., c_L appears to be small in

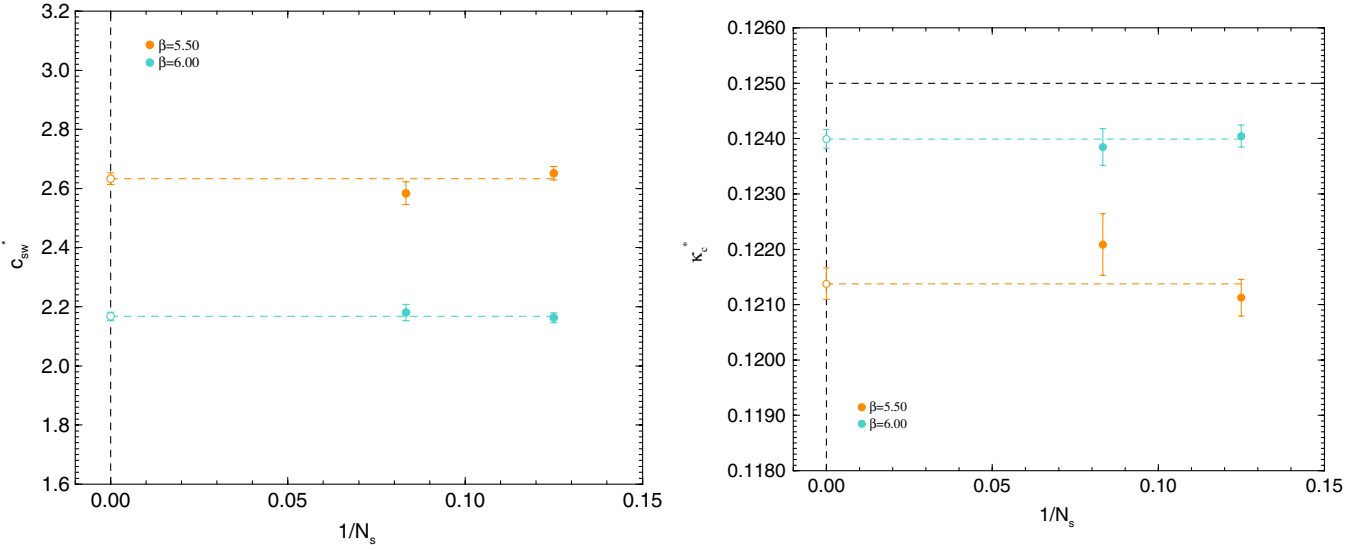


FIG. 10 (color online). c_{sw}^* against $1/N_s$ (left picture) and κ_c^* against $1/N_s$ (right picture) for $\beta = 5.50, 6.00$, filled circles. Also shown are constant fits (dashed lines) together with the extrapolated values (open circles).

Eq. (36). So in Eq. (37) we only expect small violations of $O(a)$ improvement. We shall, in the future, just consider the $8^3 \times 16$ data.

VI. RESULTS FOR c_{sw}^* AND κ_c^*

A. Perturbative results for c_{sw}^* and κ_c^*

Before giving the nonperturbative results for c_{sw}^* and κ_c^* we first recapitulate the perturbative results. The lowest order perturbative limit has been computed for both c_{sw}^* and κ_c^* [7]. For c_{sw}^* we have

$$c_{sw}^*(g_0) = 1 + (0.196244 + 1.151888\alpha - 4.2391365\alpha^2)g_0^2, \quad (40)$$

where α is the stout smearing parameter, set equal to 0.1 here. This gives

$$c_{sw}^*(g_0) = 1 + c_1 g_0^2, \quad c_1 = 0.269041, \quad (41)$$

i.e., the smearing parameter has increased the value of c_{sw}^* (for $\alpha = 0$, we have $c_1 = 0.196244$). For $\kappa_c^*(c_{sw}, g_0)$ we have

$$\begin{aligned} \kappa_c(c_{sw}, g_0) = \frac{1}{8} [& 1 + (0.0853699 - 0.961525\alpha \\ & + 3.55806\alpha^2 - (0.025221 \\ & - 0.0787379\alpha)c_{sw} - 0.00984224c_{sw}^2)g_0^2], \end{aligned} \quad (42)$$

giving for $\alpha = 0.1$

$$\begin{aligned} \kappa_c(c_{sw}, g_0) = \frac{1}{8} [& 1 + (0.024798 - 0.0173472c_{sw} \\ & - 0.00984224c_{sw}^2)g_0^2], \end{aligned} \quad (43)$$

and finally for $c_{sw} = c_{sw}^{\text{tree}} = 1$,

$$\kappa_c^*(g_0) = \frac{1}{8} [1 + k_1 g_0^2], \quad k_1 = -0.002391. \quad (44)$$

[Note that the result for $\kappa_c(c_{sw}, g_0)$ is more general than the one given in [7] when only the result for $c_{sw} = 1$ was given.]

B. Nonperturbative results for c_{sw}^* and κ_c^*

The results for c_{sw}^* and κ_c^* against g_0^2 are plotted in Figs. 11 and 12, respectively, in the range $\beta \geq 5.10$. The lowest order perturbative limits are also shown, Eqs. (41) and (44).

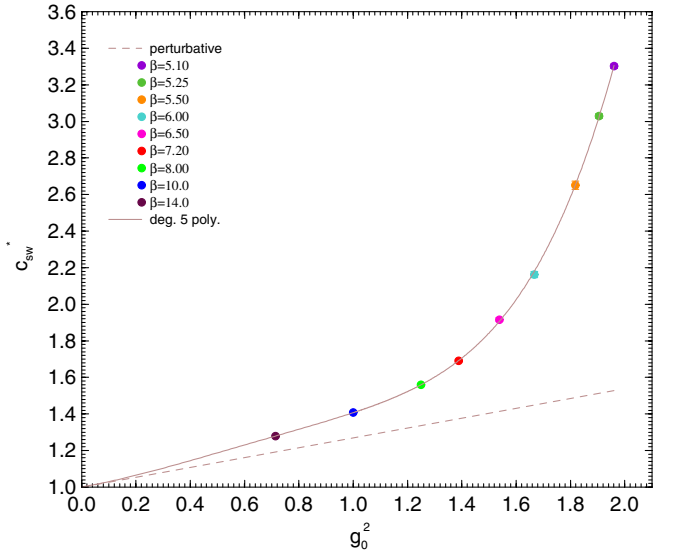


FIG. 11 (color online). c_{sw}^* against g_0^2 for various values of β (circles), together with a polynomial interpolation (line). Also shown is the perturbative result.

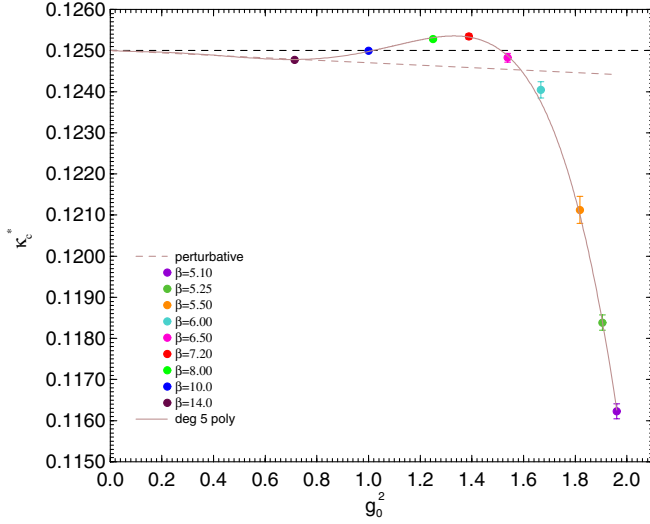


FIG. 12 (color online). κ_c^* against g_0^2 for various values of β (circles), together with a polynomial interpolation (line). Also shown is the perturbative result.

An interpolation between the numerically determined points is also shown. For both c_{sw}^* and κ_c^* a 5th order polynomial in g_0^2 proved sufficient. (These interpolation functions are constrained to reproduce the perturbative results, in the $\beta \rightarrow \infty$ limit and therefore, they have four free parameters.) For $c_{sw}^*(g_0)$ we write

$$c_{sw}^*(g_0) = 1 + c_1 g_0^2 + c_2 g_0^4 + c_3 g_0^6 + c_4 g_0^8 + c_5 g_0^{10}, \quad (45)$$

and find

$$\left. \begin{matrix} c_2 \\ c_3 \\ c_4 \\ c_5 \end{matrix} \right\} = \begin{cases} +0.299\ 10 \\ -0.114\ 91 \\ -0.200\ 03 \\ +0.153\ 59, \end{cases} \quad (46)$$

while for $\kappa_c^*(g_0)$ we write

$$\kappa_c^*(g_0) = \frac{1}{8}[1 + k_1 g_0^2 + k_2 g_0^4 + k_3 g_0^6 + k_4 g_0^8 + k_5 g_0^{10}], \quad (47)$$

and find

$$\left. \begin{matrix} k_2 \\ k_3 \\ k_4 \\ k_5 \end{matrix} \right\} = \begin{cases} +0.012\ 2470 \\ -0.052\ 5676 \\ +0.066\ 8197 \\ -0.024\ 2800. \end{cases} \quad (48)$$

These give for the specific β values used here

$$c_{sw}^* = \begin{cases} 3.306 & \beta = 5.10 \\ 3.021 & \beta = 5.25 \\ 2.653 & \beta = 5.50 \\ 2.179 & \beta = 6.00 \\ 1.907 & \beta = 6.50 \\ 1.692 & \beta = 7.20 \\ 1.560 & \beta = 8.00 \\ 1.407 & \beta = 10.0 \\ 1.279 & \beta = 14.0, \end{cases} \quad (49)$$

$$\kappa_c^* = \begin{cases} 0.116\ 262 & \beta = 5.10 \\ 0.118\ 424 & \beta = 5.25 \\ 0.120\ 996 & \beta = 5.50 \\ 0.123\ 751 & \beta = 6.00 \\ 0.124\ 870 & \beta = 6.50 \\ 0.125\ 328 & \beta = 7.20 \\ 0.125\ 314 & \beta = 8.00 \\ 0.124\ 979 & \beta = 10.0 \\ 0.124\ 783 & \beta = 14.0, \end{cases}$$

which are to be compared with the numerically determined values. The errors for c_{sw}^* from the fit are estimated to be about 0.4% while for κ_c^* we have 0.02% at $\beta = 14.0$ rising to 0.15% at $\beta = 5.10$.

These smooth fits between the points give estimates for c_{sw}^* (and κ_c^*) which could be used in the action for future generation of configurations.

For c_{sw}^* the polynomial only tracks the perturbative solution for small values of g_0^2 . This is perhaps not surprising as the tadpole improved, TI, estimate is $c_{sw}^{TI} = u_0^{(S)}/u_0^4$ [7], which is to be compared with the unsmear case of $c_{sw}^{TI} = 1/u_0^3$, where u_0 is the average plaquette value and $u_0^{(S)}$ is the smeared value. As smearing increases the plaquette value this indicates that c_{sw}^* can be large. For κ_c^* , on the other hand, as $\kappa_c^{TI} = 1/(8u_0^{(S)})$ we expect that it is $\sim 1/8$. This is true for reasonably fine lattices, however κ_c^* does begin to decrease for larger values of g_0^2 . For $n_f = 2$ the same phenomenon occurs: for larger g_0^2 , κ_c^* begins to decrease (after initially increasing).

As a further consistency check on the results, we can investigate the gradient $\partial(1/\kappa_c)/\partial c_{sw}|_{c_{sw}^*}$. From Eq. (34) we have

$$\left. \frac{\partial(1/\kappa_c)}{\partial c_{sw}} \right|_{c_{sw}^*} = d, \quad (50)$$

as the fits in Fig. 9 are linear, where d is given in Eq. (35). Perturbatively we have from Eq. (43),

$$\frac{\partial(1/\kappa_c)}{\partial c_{sw}} = 8[0.037\ 032 + 0.019\ 684(c_{sw} - 1)]g_0^2. \quad (51)$$

As g_0 increases c_{sw} increases, so not only do more terms in this expansion become important, but the coefficient of the leading term increases as well. For $c_{sw} = c_{sw}^{tree} = 1$ we

have the leading order perturbative result,

$$\left. \frac{\partial(1/\kappa_c)}{\partial c_{sw}} \right|_{c_{sw}^*} = d_1 g_0^2, \quad d_1 = 0.296\,253. \quad (52)$$

In Fig. 13 we plot $\partial(1/\kappa_c)/\partial c_{sw}|_{c_{sw}^*}$ against g_0^2 , together with a 5th order polynomial in g_0^2 ,

$$\left. \frac{\partial(1/\kappa_c)}{\partial c_{sw}} \right|_{c_{sw}^*} = d_1 g_0^2 + d_2 g_0^4 + d_3 g_0^6 + d_4 g_0^8 + d_5 g_0^{10}, \quad (53)$$

and find

$$\left. \begin{array}{l} d_2 \\ d_3 \\ d_4 \\ d_5 \end{array} \right\} = \left\{ \begin{array}{l} +0.4180 \\ -0.7232 \\ +0.4739 \\ -0.0919. \end{array} \right. \quad (54)$$

The results follow a smooth curve.

VII. CONCLUSIONS AND DISCUSSION

Nonperturbative $O(a)$ improvement is a viable procedure for (stout) smeared actions with typical clover results being obtained. (Other recent results for 3 flavors are given in [15–17].) Using the Schrödinger functional method we have determined the optimal clover coefficient c_{sw}^* , necessary to achieve $O(a)$ improvement and also the optimal critical hopping parameter, κ_c^* , Eqs. (45) and (47) over a wide range of coupling constant.

As a increases we need a significant $c_{sw} \gg c_{sw}^{\text{tree}} \equiv 1$ for $O(a)$ improvement. We are now seeking a region where $a \sim 0.05\text{--}0.1$ fm. Improvement, which is presumably represented by an asymptotic series, brings an advantage for smaller a , say $a \leq 0.1$ fm. The two extremes for a are

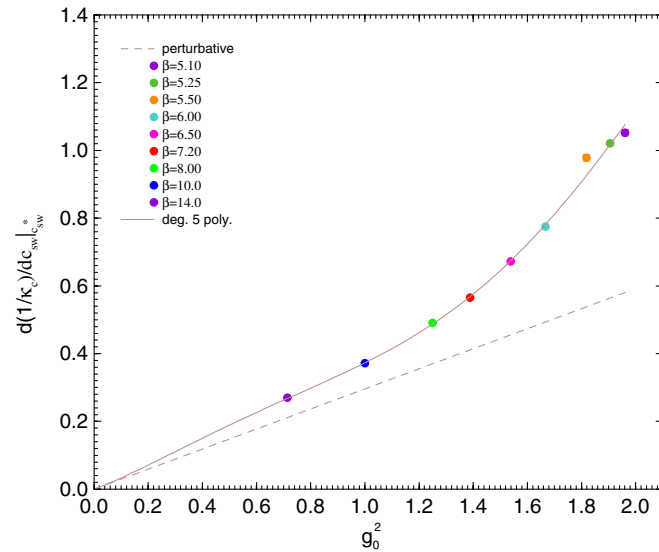


FIG. 13 (color online). $\partial(1/\kappa_c)/\partial c_{sw}|_{c_{sw}^*}$ against g_0^2 for various values of β (circles), together with a polynomial interpolation (line). Also shown is the perturbative result.

simulations at small a with “large” m_{ps} when there is no continuum extrapolation but a chiral extrapolation, or alternatively simulations at “coarse” a with $m_{ps} \sim m_\pi$ when there is no chiral extrapolation but a continuum extrapolation. Of course the Schrödinger functional does not tell us a ; for this conventional HMC simulations are required. Some preliminary results indicate that around $\beta \sim 5.50$ we have $a \sim 0.08$ fm.

ACKNOWLEDGMENTS

The numerical calculations have been performed on the BlueGeneLs at EPCC (Edinburgh, UK), NIC (Jülich, Germany), the QCDOC (Edinburgh, UK), and the SGI ICE at HLRN (Berlin-Hannover, Germany). We thank all institutions for their support. The Chroma software library was used, [20], and we are grateful to R. G. Edwards and B. Joó for their help and advice. The BLUEGENE and QCDOC codes were optimized using BAGEL, [24]. This work has been supported in part by the EU Integrated Infrastructure Initiative Hadron Physics (I3HP) under Contract No. RII3-CT-2004-506078, by the DFG under Contracts No. FOR 465 (Forschergruppe Gitter-Hadronen-Phänomenologie) and No. SFB/TR 55 (Hadron Physics from Lattice QCD) and the HPC-EUROPA++ project (Project No. 211437), funded by the European Community’s Research Infrastructure Action within the FP7 “Coordination and support action” Programme. J. M. Z. acknowledges support from STFC Grant No. PP/F009658/1.

APPENDIX: M AND ΔM RESULTS

In Tables I, II, III, IV, V, VI, VII, VIII, and IX we collect the numerical values of M and ΔM as defined in Eq. (27) for the $N_s^3 \times 2N_s = 8^3 \times 16$ lattices, while in Tables X and XI the results for the $12^3 \times 24$ lattices are given.

The data sets are of size $O(3000)$ trajectories for the $8^3 \times 16$ lattices and $O(2000)$ trajectories for the $12^3 \times 24$

TABLE I. $8^3 \times 16$ results for M and ΔM for $\beta = 5.10$.

β	c_{sw}	κ	M	ΔM
5.10	3.20	0.117 60	0.007 049(2313)	0.005 762(1923)
5.10	3.20	0.117 80	−0.013 15(205)	0.001 565(1545)
5.10	3.20	0.118 00	−0.023 24(231)	0.003 037(1212)
5.10	3.20	0.118 20	−0.041 87(212)	−0.001 353(1782)
5.10	3.30	0.116 10	0.019 41(227)	0.004 648(1570)
5.10	3.30	0.116 20	0.001 408(2298)	−0.003 942(1737)
5.10	3.30	0.116 40	−0.005 654(2058)	0.001 279(1438)
5.10	3.30	0.116 60	−0.025 96(166)	−0.002 347(1310)
5.10	3.30	0.116 90	−0.043 56(181)	−0.004 137(1550)
5.10	3.40	0.114 70	0.010 98(191)	−0.003 299(1305)
5.10	3.40	0.114 90	−0.004 606(1516)	−0.004 438(1044)
5.10	3.40	0.115 10	−0.017 42(160)	−0.006 135(1442)
5.10	3.40	0.115 30	−0.024 32(125)	−0.005 855(748)
5.10	3.40	0.115 50	−0.034 24(165)	−0.004 780(1086)

TABLE II. $8^3 \times 16$ results for M and ΔM for $\beta = 5.25$.

β	c_{sw}	κ	M	ΔM
5.25	2.90	0.120 00	0.027 72(322)	0.007 506(2096)
5.25	2.90	0.120 15	0.014 68(226)	0.008 527(1944)
5.25	2.90	0.120 25	0.005 850(2967)	0.003 412(1559)
5.25	2.90	0.120 50	-0.020 97(186)	0.004 020(1167)
5.25	2.90	0.121 00	-0.049 47(241)	0.000 895 2(14 184)
5.25	3.00	0.118 60	0.020 41(279)	-0.000 731 9(14 965)
5.25	3.00	0.118 75	0.000 855 6(19 694)	0.001 173(1115)
5.25	3.00	0.118 90	-0.006 210(2160)	-0.001 295(1424)
5.25	3.00	0.119 05	-0.017 27(244)	-0.006 479(2808)
5.25	3.00	0.119 20	-0.032 80(169)	-0.002 655(1102)
5.25	3.10	0.117 00	0.019 73(153)	-0.001 642(991)
5.25	3.10	0.117 20	0.010 21(171)	-0.002 551(1054)
5.25	3.10	0.117 40	-0.002 194(1506)	-0.001 440(922)
5.25	3.10	0.117 60	-0.013 03(133)	-0.002 512(1050)
5.25	3.10	0.117 80	-0.023 44(186)	-0.000 873 2(12 753)
5.25	3.20	0.115 80	0.010 19(131)	-0.005 591(815)
5.25	3.20	0.116 00	0.000 167 3(11 516)	-0.005 485(875)
5.25	3.20	0.116 20	-0.008 058(1185)	-0.005 259(1342)
5.25	3.20	0.116 40	-0.019 05(114)	-0.003 621(1214)

TABLE III. $8^3 \times 16$ results for M and ΔM for $\beta = 5.50$.

β	c_{sw}	κ	M	ΔM
5.50	2.50	0.123 00	0.026 08(208)	0.005 685(1134)
5.50	2.50	0.123 20	0.011 12(215)	0.003 630(1484)
5.50	2.50	0.123 35	-0.001 449(2014)	0.004 018(1567)
5.50	2.50	0.123 60	-0.015 65(210)	0.007 337(1321)
5.50	2.60	0.121 70	0.006 007(1703)	0.000 970 0(16 220)
5.50	2.60	0.121 90	-0.000 161 4(18 320)	0.001 739(1046)
5.50	2.60	0.122 10	-0.013 43(170)	0.000 162 8(11 051)
5.50	2.60	0.122 30	-0.019 59(223)	0.003 397(1508)
5.50	2.70	0.120 15	0.015 84(149)	-0.002 008(1139)
5.50	2.70	0.120 40	0.002 419(1200)	-0.001 062(798)
5.50	2.70	0.120 70	-0.012 64(125)	-0.001 321(1175)
5.50	2.70	0.120 90	-0.018 31(150)	-0.001 626(915)

TABLE IV. $8^3 \times 16$ results for M and ΔM for $\beta = 6.00$.

β	c_{sw}	κ	M	ΔM
6.00	2.10	0.124 30	0.018 41(99)	0.001 623(800)
6.00	2.10	0.124 60	0.006 443(1084)	0.001 332(753)
6.00	2.10	0.124 95	-0.004 446(970)	0.000 645 2(7878)
6.00	2.10	0.125 20	-0.013 16(107)	0.003 539(970)
6.00	2.20	0.123 30	0.011 35(86)	-0.000 757 6(5905)
6.00	2.20	0.123 55	0.002 234(706)	-0.000 174 7(6084)
6.00	2.20	0.123 90	-0.010 50(79)	-0.000 806 1(7138)
6.00	2.20	0.124 20	-0.021 08(79)	-0.000 865 0(6771)
6.00	2.30	0.121 90	0.019 96(58)	-0.002 989(439)
6.00	2.30	0.122 15	0.009 817(838)	-0.002 765(574)
6.00	2.30	0.122 40	0.000 133 5(7744)	-0.003 061(672)
6.00	2.30	0.122 80	-0.014 30(67)	-0.003 268(549)
6.00	2.40	0.121 00	0.012 28(69)	-0.004 705(456)
6.00	2.40	0.121 20	0.003 415(610)	-0.005 526(586)
6.00	2.40	0.121 40	-0.004 357(723)	-0.004 751(540)
6.00	2.40	0.121 60	-0.010 66(73)	-0.004 149(657)

TABLE V. $8^3 \times 16$ results for M and ΔM for $\beta = 6.50$.

β	c_{sw}	κ	M	ΔM
6.50	1.80	0.125 50	0.019 94(59)	0.001 612(472)
6.50	1.80	0.125 75	0.010 67(59)	0.001 914(457)
6.50	1.80	0.126 00	0.001 513(513)	0.001 973(466)
6.50	1.80	0.126 50	-0.016 00(55)	0.002 172(496)
6.50	1.90	0.124 40	0.021 39(60)	0.000 403 9(4011)
6.50	1.90	0.124 70	0.010 68(56)	0.001 113(435)
6.50	1.90	0.124 95	0.001 754(539)	0.000 338 8(5215)
6.50	1.90	0.125 20	-0.007 849(601)	-0.000 030 26(52 328)
6.50	2.00	0.123 60	0.012 55(49)	-0.002 074(450)
6.50	2.00	0.123 90	0.001 931(525)	-0.001 253(358)
6.50	2.00	0.124 10	-0.006 006(505)	-0.002 711(510)
6.50	2.00	0.124 40	-0.016 35(49)	-0.001 294(453)

lattices. An initial thermalization phase was typically of order 300 trajectories. The trajectory length τ_{chroma} was always 1, while the number of steps in the trajectory, $n_{\tau_{\text{chroma}}}$, varied for the $8^3 \times 16$ lattices from 10 for $\beta \geq 6.50$ to 12, 12, 15, and 18 for $\beta = 6.00, 5.50, 5.25,$ and 5.10 , respectively. This maintained an acceptance rate of $>80\%$. (This decreased very slightly for the larger β values.) For the $12^3 \times 24$ lattices $n_{\tau_{\text{chroma}}} = 18, 22$ for $\beta = 6.00, 5.50$ was used to give this acceptance.

The jackknife errors for the ratios are given uniformly to two significant figures, with the overriding requirement that the result must also have a minimum of four significant figures. To reduce possible autocorrelations in the data every second trajectory was used with a jackknife block size of 10.

TABLE VI. $8^3 \times 16$ results for M and ΔM for $\beta = 7.20$.

β	c_{sw}	κ	M	ΔM
7.20	1.40	0.127 20	0.025 34(46)	0.006 503(387)
7.20	1.40	0.127 97	-0.000 759 7(4109)	0.005 029(430)
7.20	1.40	0.128 50	-0.017 13(48)	0.005 118(372)
7.20	1.40	0.129 20	-0.039 70(53)	0.007 053(563)
7.20	1.60	0.125 00	0.038 39(43)	0.003 053(391)
7.20	1.60	0.125 70	0.015 00(38)	0.001 534(389)
7.20	1.60	0.126 15	0.000 339 1(4484)	0.001 883(311)
7.20	1.60	0.126 60	-0.015 25(36)	0.001 353(543)
7.20	1.60	0.127 20	-0.036 08(38)	0.001 644(307)
7.20	1.80	0.122 70	0.056 07(29)	-0.001 786(239)
7.20	1.80	0.123 80	0.019 59(32)	-0.001 553(260)
7.20	1.80	0.124 38	-0.000 080 70(34 186)	-0.002 103(288)
7.20	1.80	0.125 00	-0.021 36(34)	-0.001 939(300)
7.20	1.80	0.125 90	-0.053 19(35)	-0.001 455(388)
7.20	2.00	0.121 50	0.038 19(31)	-0.005 604(315)
7.20	2.00	0.122 10	0.017 36(38)	-0.005 245(340)
7.20	2.00	0.122 64	-0.000 202 7(3196)	-0.005 262(470)
7.20	2.00	0.122 90	-0.008 518(356)	-0.005 990(375)
7.20	2.00	0.123 60	-0.034 21(34)	-0.006 188(311)

TABLE VII. $8^3 \times 16$ results for M and ΔM for $\beta = 8.00$.

β	c_{sw}	κ	M	ΔM
8.00	1.40	0.125 70	0.027 42(25)	0.003 117(207)
8.00	1.40	0.126 30	0.007 469(239)	0.002 932(272)
8.00	1.40	0.126 51	0.000 197 1(2329)	0.002 716(221)
8.00	1.40	0.126 80	-0.009 671(223)	0.003 270(247)
8.00	1.40	0.127 30	-0.025 96(28)	0.003 221(256)
8.00	1.60	0.124 30	0.022 66(23)	-0.000 497 2(2019)
8.00	1.60	0.124 80	0.005 679(245)	-0.000 871 8(2676)
8.00	1.60	0.124 98	0.000 248 4(2335)	-0.000 860 8(2491)
8.00	1.60	0.125 20	-0.007 169(242)	-0.000 600 4(2378)
8.00	1.60	0.125 70	-0.024 10(25)	-0.001 201(239)
8.00	1.80	0.122 40	0.035 01(24)	-0.003 785(264)
8.00	1.80	0.122 90	0.018 58(26)	-0.003 763(179)
8.00	1.80	0.123 44	0.000 595 9(2472)	-0.004 154(247)
8.00	1.80	0.123 50	-0.002 196(264)	-0.005 071(223)
8.00	1.80	0.124 00	-0.018 61(27)	-0.004 060(270)

TABLE X. $12^3 \times 24$ results for M and ΔM for $\beta = 5.50$.

β	c_{sw}	κ	M	ΔM
5.50	2.50	0.123 00	0.025 40(221)	0.000 615 3(17 988)
5.50	2.50	0.123 20	0.004 367(3139)	0.001 051(1568)
5.50	2.50	0.123 35	-0.002 279(2162)	0.001 425(1272)
5.50	2.50	0.123 60	-0.019 81(151)	0.002 050(1237)
5.50	2.60	0.121 70	0.007 744(2026)	-0.000 943 8(8558)
5.50	2.60	0.121 90	-0.002 810(1805)	0.000 240 7(11 134)
5.50	2.60	0.122 10	-0.011 17(179)	-0.000 847 1(12 790)
5.50	2.60	0.122 30	-0.025 60(168)	-0.000 741 6(19 293)
5.50	2.70	0.120 15	0.012 89(175)	-0.000 896 7(10 745)
5.50	2.70	0.120 40	0.001 170(2838)	-0.000 306 2(16 169)
5.50	2.70	0.120 70	-0.012 24(140)	-0.001 362(852)
5.50	2.70	0.120 90	-0.021 38(153)	0.000 267 7(9645)

TABLE VIII. $8^3 \times 16$ results for M and ΔM for $\beta = 10.00$.

β	c_{sw}	κ	M	ΔM
10.00	1.20	0.125 70	0.016 41(22)	0.003 409(179)
10.00	1.20	0.126 19	-0.000 130 6(1605)	0.003 338(182)
10.00	1.20	0.126 30	-0.003 541(173)	0.003 321(217)
10.00	1.20	0.126 90	-0.023 50(20)	0.003 296(198)
10.00	1.20	0.127 50	-0.043 40(17)	0.003 247(206)
10.00	1.40	0.124 10	0.030 94(21)	0.000 344 2(1695)
10.00	1.40	0.124 70	0.013 51(29)	0.000 686 0(2239)
10.00	1.40	0.125 07	0.000 456 3(4134)	0.001 032(171)
10.00	1.40	0.125 30	-0.008 549(319)	0.000 568 3(2022)
10.00	1.40	0.125 90	-0.027 94(27)	0.001 172(222)
10.00	1.60	0.122 70	0.033 42(46)	-0.004 086(267)
10.00	1.60	0.123 20	0.021 52(16)	-0.003 744(145)
10.00	1.60	0.123 82	0.001 171(165)	-0.003 759(157)
10.00	1.60	0.123 90	-0.002 455(294)	-0.003 601(186)
10.00	1.60	0.124 50	-0.021 61(19)	-0.004 090(163)

TABLE IX. $8^3 \times 16$ results for M and ΔM for $\beta = 14.00$.

β	c_{sw}	κ	M	ΔM
14.00	1.10	0.125 00	0.017 23(8)	0.002 646(110)
14.00	1.10	0.125 30	0.007 452(89)	0.002 787(103)
14.00	1.10	0.125 60	-0.002 273(87)	0.002 941(114)
14.00	1.10	0.125 90	-0.011 96(9)	0.002 676(100)
14.00	1.10	0.126 20	-0.021 94(9)	0.002 684(113)
14.00	1.20	0.124 20	0.032 18(36)	0.001 696(167)
14.00	1.20	0.124 70	0.014 23(16)	0.001 044(98)
14.00	1.20	0.125 30	-0.002 225(329)	0.002 191(174)
14.00	1.20	0.125 80	-0.017 86(46)	0.002 320(199)
14.00	1.30	0.123 80	0.029 00(34)	-0.001 514(170)
14.00	1.30	0.124 30	0.011 32(40)	-0.000 489 4(1641)
14.00	1.30	0.124 80	-0.005 572(301)	-0.000 739 2(1529)
14.00	1.30	0.125 30	-0.020 27(107)	-0.000 980 7(2838)

TABLE XI. $12^3 \times 24$ results for M and ΔM for $\beta = 6.00$.

β	c_{sw}	κ	M	ΔM
6.00	2.10	0.124 30	0.019 57(74)	0.000 362 9(5316)
6.00	2.10	0.124 60	0.007 496(680)	0.000 620 2(5838)
6.00	2.10	0.124 95	-0.001 642(1038)	0.001 463(1070)
6.00	2.10	0.125 20	-0.011 23(113)	0.000 541 1(5241)
6.00	2.20	0.123 30	0.012 28(67)	-0.000 830 8(5383)
6.00	2.20	0.123 55	0.002 046(917)	-0.000 895 3(4855)
6.00	2.20	0.123 90	-0.011 53(83)	0.000 513 9(5375)
6.00	2.20	0.124 20	-0.020 19(76)	-0.000 312 9(6525)
6.00	2.30	0.121 90	0.021 11(49)	-0.001 234(455)
6.00	2.30	0.122 15	0.010 67(68)	-0.001 233(833)
6.00	2.30	0.122 40	0.002 555(557)	-0.000 873 5(5407)
6.00	2.30	0.122 80	-0.013 06(64)	-0.000 156 5(5009)
6.00	2.40	0.121 00	0.012 73(49)	-0.001 217(461)
6.00	2.40	0.121 20	0.005 458(635)	-0.002 194(415)
6.00	2.40	0.121 40	-0.003 718(533)	-0.002 257(514)
6.00	2.40	0.121 60	-0.009 398(475)	-0.001 493(486)

- [1] B. Sheikholeslami and R. Wohlert, Nucl. Phys. **B259**, 572 (1985).
- [2] M. Lüscher, S. Sint, R. Sommer, and P. Weisz, Nucl. Phys. **B478**, 365 (1996).
- [3] C. Morningstar and M.J. Peardon, Phys. Rev. D **69**, 054501 (2004).
- [4] S. Capitani, S. Dürr, and C. Hoelbling, J. High Energy Phys. **11** (2006) 028.
- [5] T.A. DeGrand, A. Hasenfratz, and T.G. Kovács, Nucl. Phys. **B547**, 259 (1999).
- [6] S. Boinepalli, W. Kamleh, D.B. Leinweber, A.G. Williams, and J.M. Zanotti, Phys. Lett. B **616**, 196 (2005).
- [7] R. Horsley, H. Perlt, P.E.L. Rakow, G. Schierholz, and A. Schiller (QCDSF Collaboration), Phys. Rev. D **78**, 054504 (2008); Proc. Sci., LATTICE2008 (2008) 164 [arXiv:hep-lat/0809.4769].
- [8] S. Aoki, M. Fukugita, S. Hashimoto, K-I. Ishikawa, N. Ishizuka, Y. Iwasaki, K. Kanaya, T. Kaneko, Y. Kuramashi, M. Okawa, N. Tsutsui, A. Ukawa, N. Yamada, and T. Yoshié (JLQCD Collaboration), Phys. Rev. D **72**, 054510 (2005).
- [9] M. Lüscher, R. Narayanan, P. Weisz, and U. Wolff, Nucl. Phys. **B384**, 168 (1992).
- [10] S. Sint, Nucl. Phys. **B421**, 135 (1994).
- [11] S. Sint, Nucl. Phys. **B451**, 416 (1995).
- [12] M. Lüscher, S. Sint, R. Sommer, P. Weisz, and U. Wolff, Nucl. Phys. **B491**, 323 (1997).
- [13] R. G. Edwards, U. M. Heller, and T. R. Klassen, Phys. Rev. Lett. **80**, 3448 (1998).
- [14] K. Jansen and R. Sommer, Nucl. Phys. **B530**, 185 (1998); **643**, 517(E) (2002).
- [15] N. Yamada, S. Aoki, M. Fukugita, S. Hashimoto, K-I. Ishikawa, N. Ishizuka, Y. Iwasaki, K. Kanaya, T. Kaneko, Y. Kuramashi, M. Okawa, Y. Taniguchi, N. Tsutsui, A. Ukawa, and T. Yoshié (CP-PACS, JLQCD Collaborations), Phys. Rev. D **71**, 054505 (2005).
- [16] S. Aoki, M. Fukugita, S. Hashimoto, K-I. Ishikawa, N. Ishizuka, Y. Iwasaki, K. Kanaya, T. Kaneko, Y. Kuramashi, M. Okawa, S. Takeda, Y. Taniguchi, N. Tsutsui, A. Ukawa, N. Yamada, and T. Yoshié (CP-PACS, JLQCD Collaborations), Phys. Rev. D **73**, 034501 (2006).
- [17] R. G. Edwards, B. Joó, and H.-W. Lin, Phys. Rev. D **78**, 054501 (2008).
- [18] T. Klassen, Nucl. Phys. **B509**, 391 (1998).
- [19] S. Aoki, R. Frezzotti, and P. Weisz, Nucl. Phys. **B540**, 501 (1999).
- [20] R. G. Edwards and B. Joó, Nucl. Phys. B, Proc. Suppl. **140**, 832 (2005).
- [21] M. A. Clark and A. D. Kennedy, Phys. Rev. Lett. **98**, 051601 (2007).
- [22] N. Cundy, M. Göckeler, R. Horsley, T. Kaltenbrunner, A. D. Kennedy, Y. Nakamura, H. Perlt, D. Pleiter, P. E. L. Rakow, A. Schäfer, G. Schierholz, A. Schiller, H. Stüben, and J. M. Zanotti (QCDSF-UKQCD Collaboration), Proc. Sci., LATTICE2008 (2008) 132 [arXiv:hep-lat/0811.2355].
- [23] M. Lüscher and P. Weisz, Nucl. Phys. **B479**, 429 (1996).
- [24] P. A. Boyle, <http://www.ph.ed.ac.uk/~paboyle/bagel/Bagel.html> (2005).